

Chandra observations of the planetary nebula IC 4593

J.A. Toalá^{1*}, M.A. Guerrero², L. Bianchi³, Y.-H. Chu⁴ and O. De Marco⁵

¹Instituto de Radioastronomía y Astrofísica (IRyA), UNAM Campus Morelia, Apartado postal 3-72, 58090 Morelia, Michoacan, Mexico

²Instituto de Astrofísica de Andalucía (IAA-CSIC), Glorieta de la Astronomía S/N, 18008 Granada, Spain

³Department of Physics and Astronomy, The Johns Hopkins University, Baltimore, MD, USA

⁴Institute of Astronomy and Astrophysics, Academia Sinica (ASIAA), Taipei 10617, Taiwan, Republic of China

⁵Astronomy, Astrophysics and Astrophotonics Research Centre, Macquarie University, Sydney, NSW 2109, Australia

10 April 2020

ABSTRACT

The ACIS-S camera on board the *Chandra X-ray Observatory* has been used to discover a hot bubble in the planetary nebula (PN) IC 4593, the most distant PN detected by *Chandra* so far. The data are used to study the distribution of the X-ray-emitting gas in IC 4593 and to estimate its physical properties. The hot bubble has a radius of $\sim 2''$ and is found to be confined inside the optically-bright innermost cavity of IC 4593. The X-ray emission is mostly consistent with that of an optically-thin plasma with temperature $kT \approx 0.15$ keV (or $T_X \approx 1.7 \times 10^6$ K), electron density $n_e \approx 15 \text{ cm}^{-3}$, and intrinsic X-ray luminosity in the 0.3–1.5 keV energy range $L_X = 3.4 \times 10^{30} \text{ erg s}^{-1}$. A careful analysis of the distribution of hard ($E > 0.8$ keV) photons in IC 4593 suggests the presence of X-ray emission from a point source likely associated with its central star (CSPN). If this were the case, its estimated X-ray luminosity would be $L_{X,\text{CSPN}} = 7 \times 10^{29} \text{ erg s}^{-1}$, fulfilling the $\log(L_{X,\text{CSPN}}/L_{\text{bol}}) \approx -7$ relation for self-shocking winds in hot stars. The X-ray detection of the CSPN helps explain the presence of high-ionisation species detected in the UV spectra as predicted by stellar atmosphere models.

Key words: (ISM:) planetary nebulae: general – (ISM:) planetary nebulae: IC 4593 – Stars: winds, outflows – Stars: low-mass – X-rays: general

1 INTRODUCTION

The unprecedented angular resolution of the *Chandra X-ray Observatory* has revealed in exquisite detail the hot interiors of planetary nebulae (PNe). The first *Chandra* observations of PNe already revealed that hot bubbles are contained within their inner rims (see the cases of BD+30°3639 and NGC 6543; Kastner et al. 2000; Chu et al. 2001). These hot bubbles form as the result of interactions of the fast wind from the central star (CSPN) with material ejected during the previous asymptotic giant branch (AGB) phase. This wind-wind interaction creates an adiabatically-shocked region or hot bubble with temperatures that are determined by the CSPN terminal wind velocity as $T \sim v_\infty^2$ (Dyson & Williams 1997). Typical wind velocities from CSPN are reported to be $v_\infty \gtrsim 500 - 4000 \text{ km s}^{-1}$ (e.g., Guerrero & De Marco 2013), producing shocked plasma at X-ray-emitting temperatures in excess of 10^6 K. These general X-ray properties of hot bubbles in PNe have been largely confirmed by the *Chandra* Planetary Nebula Survey (ChanPlaNS; Kastner et al. 2012; Freeman et al. 2014), a volume-limited survey of a sample of nearby ($d < 1.5$ kpc) PNe. Extended X-ray emission has a detection rate among PNe $\sim 30\%$, with particularly high prevalence among compact ($r < 0.2$ pc) PNe with closed-shell morphology.

Chandra has also unveiled unexpected point-sources of hard X-ray emission (> 0.5 keV) from CSPNe (Guerrero et al. 2001), whose presence in a significant number of them has been confirmed by ChanPlaNS (Montez et al. 2015). Whereas some of these hard X-ray sources can be attributed to the coronal emission from a dwarf or giant late-type companion (Montez et al. 2010) or even to accretion onto a compact companion (Guerrero et al. 2019), shocks in fast winds as in OB and Wolf-Rayet stars can also be the cause of this hard X-ray emission (Guerrero et al. 2001), especially among CSPNe with powerful fast stellar winds. As these stellar winds are radiatively driven and thus inherently unstable, small-scale inhomogeneities can lead to strong stochastic shocks within the dense wind layers and heat material to X-ray-emitting temperatures (Lucy & White 1980; Gayley & Owocki 1995). Single OB stars are typically detected in X-rays ($L_X = 10^{31} - 10^{33} \text{ ergs s}^{-1}$, $kT = 0.2 - 0.5$ keV) with X-ray to bolometric luminosity ratios $L_X/L_{\text{bol}} \sim 10^{-7}$ (Berghoefer et al. 1997; Sana et al. 2006; Nebot Gómez-Morán & Oskinova 2018).

Further evidence for wind shocks in OB stars is provided by P-Cygni profiles of the so-called super-ions, species with ionisation potentials (IP) well above that of He II (IP=54.4 eV). Super-ions in OB stars cannot be abundantly produced by photo-ionisation because the stellar continuum shortwards of 228 Å is largely absorbed by He I for bound-free transitions. Thus, Auger ionisations

* E-mail: j.toala@irya.unam.mx

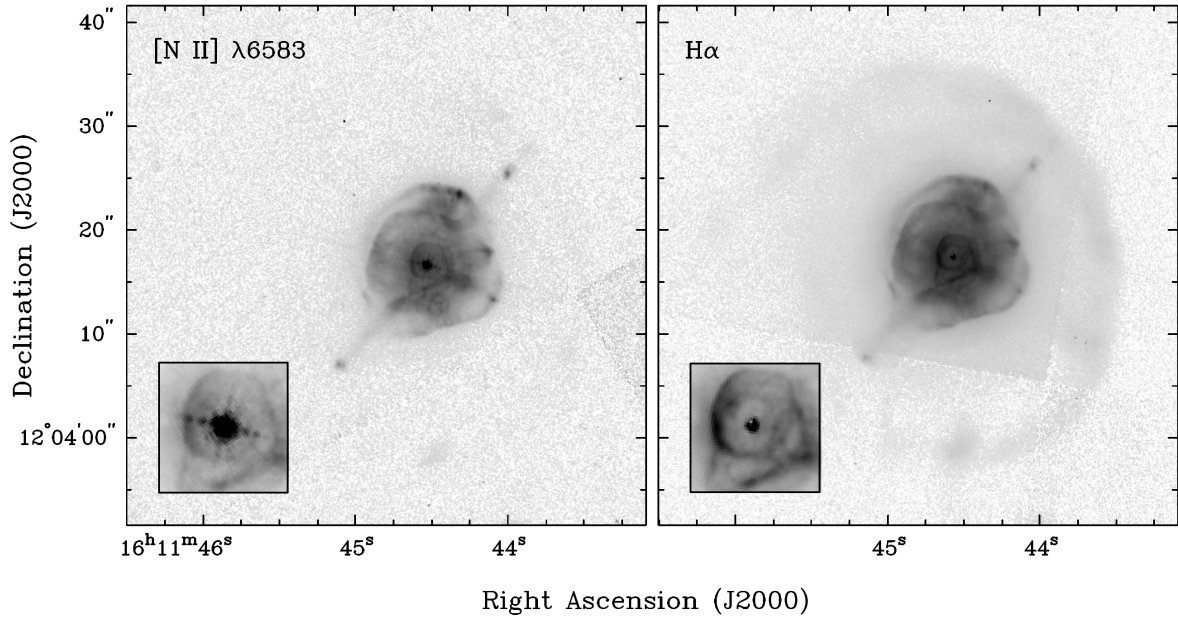


Figure 1. *HST* WFPC2 [N II] $\lambda 6583$ (left) and $H\alpha$ (right) images of the main nebular region of IC 4593. The inset shows the innermost $5'' \times 5''$ region.

by X-ray photons generated by wind shocks provide the only plausible mechanism to produce super-ions (Cassinelli & Olson 1979). Detailed modeling of UV and optical spectra of H-rich CSPNe indeed indicates that the inclusion of X-rays in the model atmosphere calculation is absolutely necessary to reproduce with a uniquely consistent effective temperature the S vI (IP of S v = 72.6 eV), N v (IP of N v = 77.5 eV), and O vI (IP of O v = 113.9 eV) doublets for stars with $T_{\text{eff}} \leq 45,000$ K, while it improves the spectral fit for stars with $T_{\text{eff}} = 55,000\text{--}80,000$ K (Herald & Bianchi 2011). Among the stars with these spectral properties, the CSPN of IC 4593 stands out for its noticeable O vI P Cygni profiles ($v_{\infty} = 1,150$ km s $^{-1}$) and low effective temperature, $\approx 41,000$ K. It also stands out for its wind variability, detected both in *IUE* (Patriarchi & Perinotto 1995) and *FUSE* (Guerrero & De Marco 2013) spectra, with ripples moving bluewards in the troughs of P Cygni profiles in various UV lines with timescales of a few hours similar to those of its pervasive optical lines (De Marco et al. 2004) and photometric variations (Miszalski et al. 2009).

IC 4593 exhibits a complex optical multiple-shell morphology with a roughly elliptical inner rim with average radius $\sim 2''$, a roundish bright filamentary outer shell $\sim 16''$ in size, two prominent jet-like features protruding from the inner shell towards NW and SE, and an asymmetrical arc-like outer shell that extends $\sim 20''$ from the CSPN. In addition to this main jet-like feature, there are others aligned along different directions, which seem to be stagnated at the edge of the shell, as implied by their negligible systemic velocities (Corradi et al. 1997). All these features can be appreciated in Figure 1. Furthermore, there is an additional halo $\sim 130'' \times 120''$ in size (see figure 2 in Corradi et al. 1997), whose fragmented and asymmetrical morphology is indicative of interaction with the interstellar medium (see Zucker & Soker 1993; Villaver et al. 2003, 2012).

The complex morphology of the main nebula of IC 4593 is suggestive of the action of different shaping agents. The current fast stellar wind would be responsible of the formation of the inner rim, whereas the collimated outflows protruding along different direc-

tions (Corradi et al. 1997; O’Connor et al. 1999) would shape the outer shell. Actually, Corradi et al. (1997) suggest that the inner rim might have been pierced by the jets ending with the pair of knots aligned along the SE-NW direction, which may be associated with bipolar jets, although this would require an inclination angle of the outflow with respect to the plane of the sky $\leq 15^\circ$ because no kinematical signature is detected in their high-dispersion spectra. Episodic rotating jets would be a natural consequence of a precessing accretion disk around a binary companion, as expected after the evolution of a binary system through a common envelope phase (see Zou et al. 2019, and references therein). Indeed, the presence of a binary system at the core of IC 4593 has been suggested through radial velocity measurements of absorption lines of He II (e.g., De Marco et al. 2004) making this system a candidate for binary interactions and for the emission of X-rays from the coronal activity of a dwarf late-type companion.

Here we present Cycle 13 *Chandra* ACIS-S observations of IC 4593, which was not originally included in the ChanPlaNS sample because of its large distance, $d = 2.4_{-0.4}^{+0.6}$ kpc (Bailer-Jones et al. 2018). We use our *Chandra* observations to unveil the presence of extended X-ray emission within IC 4593 and to search for possible X-ray emission from its central star or a binary companion. The paper is organized as follows: the observations and data analysis are presented in Section 2, the results discussed in Section 3, and a summary presented in Section 4.

2 OBSERVATIONS AND DATA ANALYSIS

IC 4593 was observed by *Chandra* on 2012 January 2 during Cycle 13 (PI: M.A. Guerrero; Obs. ID. 13654). The observations were performed with the back-illuminated CCD 3 of the ACIS-S array in the VFaint mode for a total exposure time of 80 ks. After processing the data with the *Chandra* Interactive Analysis of Observations (CIAO; version 4.9; Fruscione et al. 2006), the resulted total useful time is 76.3 ks. There were no periods of time in which the data

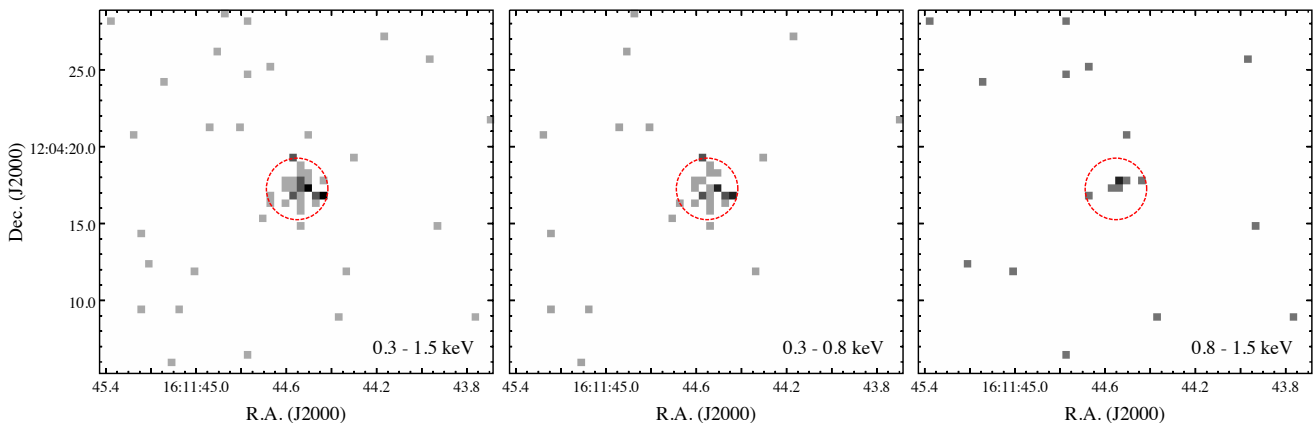


Figure 2. *Chandra* ACIS-S event images of IC 4593 in the 0.3–1.5 keV (left), 0.3–0.8 keV (center), and 0.8–1.5 keV (right) energy bands. The red dashed circle is centered on the CSPN of IC 4593 and has an angular radius of $2''$. The images have been produced using the natural ACIS-S pixel size of $0''.5$.

were affected by high-level backgrounds. The *Chandra* observations detect X-ray emission at the location of IC 4593, with a total ACIS-S3 count number of 31 ± 6 counts in the energy range 0.3–1.5 keV, which corresponds to a net ACIS-S3 count rate of 0.38 ± 0.07 counts ks^{-1} in this same energy range. We investigate next the spatial distribution and spectral properties of this X-ray emission.

2.1 Spatial properties of the X-ray emission

To examine the spatial distribution of the X-ray emission, we created an image of the X-ray events in the 0.3–1.5 keV energy range (left panel of Figure 2), which is the energy range in which most of hot bubbles in PNe have been detected (see Ruiz et al. 2013; Kastner et al. 2012, and references therein). The image, produced using the natural ACIS-S pixel size of $0''.5$, reveals the presence of extended emission spatially confined within the inner rim of IC 4593, which is represented by a circular aperture with an angular radius of $2''$.

To further confirm the spatial correspondence between the diffuse X-ray emission of IC 4593 and its optical inner rim, we created a smoothed image of the X-ray emission from IC 4593 in the 0.3–2.0 keV band using the CIAO task *aconvolve*. The image is smoothed using a circular Gaussian kernel with size up to 4 pixels ($\approx 2''$) and a fast-Fourier transform (FFT) convolution method. The final smoothed image is presented in the left panel of Figure 3 and, for comparison with the optical morphology, a color-composite image of IC 4593 using the *HST* [N II] and [O III] narrowband images and the smoothed X-ray image is presented in the right panel. Figure 3 right panel shows that the X-ray emission fills the innermost cavity of IC 4593.

2.2 Spectral properties of the X-ray emission

The spectrum of the X-ray emission from IC 4593 was extracted using the CIAO task *specextract* from a region with a radius of $2''$ enclosing the inner rim. A background spectrum was extracted from a region with no contribution from background X-ray sources. The resultant background-subtracted ACIS-S spectrum of IC 4593 is shown in Figure 4. Given the small number of counts, the spectrum quality is notably poor. Nonetheless, its spectral shape is consistent with the emission from a low-temperature optically-thin plasma typical of PN hot bubbles (Montez et al. 2005; Ruiz et al. 2013);

the spectrum is soft and peaks between 0.5–0.6 keV with apparent line emission features around ~ 0.4 keV and $\lesssim 1.0$ keV. The dominant peak can be attributed to the O VII triplet, while the emission around 0.4 keV might be due to the contribution from C IV and/or N VI lines. No emission is detected beyond 2.0 keV.

Since the data quality does not warrant a standard spectral fit using the reduced χ^2 method, we have rather qualitatively compared the observed background-subtracted spectrum with a number of synthetic *apec*¹ optically-thin plasma X-ray spectra modelled using XSPEC version 12.10.1 (Arnaud 1996). A fixed hydrogen column density $N_{\text{H}} = 4.3 \times 10^{20} \text{ cm}^{-2}$, as estimated by the NASA HEASARC N_{H} tool², was adopted as the absorption column. We note that this value is consistent with the $E(B - V)$ value of 0.06 mag reported by Herald & Bianchi (2011). A model with plasma temperature $T_{\text{X}} \lesssim 0.15$ keV (plotted in solid line in Figure 4) describes reasonably well the ACIS-S3 spectrum. Higher plasma temperatures ($T_{\text{X}} \approx 0.20$ keV) displace the dominant spectral feature at ~ 0.55 keV towards higher energies, whereas lower plasma temperatures ($T_{\text{X}} \approx 0.10$ keV) produce larger emission at lower energies. The estimated observed flux of the model is $f_{\text{X}} \approx 3.3 \times 10^{-15} \text{ erg s}^{-1} \text{ cm}^{-2}$, which corresponds to an unabsorbed X-ray flux of $F_{\text{X}} \approx 5.0 \times 10^{-15} \text{ erg s}^{-1} \text{ cm}^{-2}$ and a luminosity of $L_{\text{X}} \approx 3.4 \times 10^{30} \text{ erg s}^{-1}$. For the X-ray temperature range between 0.1 and 0.2 keV described above, models with X-ray luminosities in excess of $6 \times 10^{30} \text{ erg s}^{-1}$ and below $2 \times 10^{30} \text{ erg s}^{-1}$ result in predicted spectral shapes that deviate significantly from the observed spectrum. The normalization parameter A , estimated to be $3.9 \times 10^{-6} \text{ cm}^{-5}$, was used to derive an electron density of $n_{\text{e}} \sim 15 \text{ cm}^{-3}$ for the hot bubble in IC 4593³.

¹ A collisionally-ionised diffuse gas model calculated from the AtomDB atomic database (<http://atomdb.org/>) which is included in XSPEC.

² <https://heasarc.gsfc.nasa.gov/cgi-bin/Tools/w3nh/w3nh.pl>

³ The normalization parameter can be expressed as $A = 10^{-14} \int n_{\text{e}}^2 dV / 4\pi d^2$, where d is the distance and V is the volume of the X-ray-emitting region.

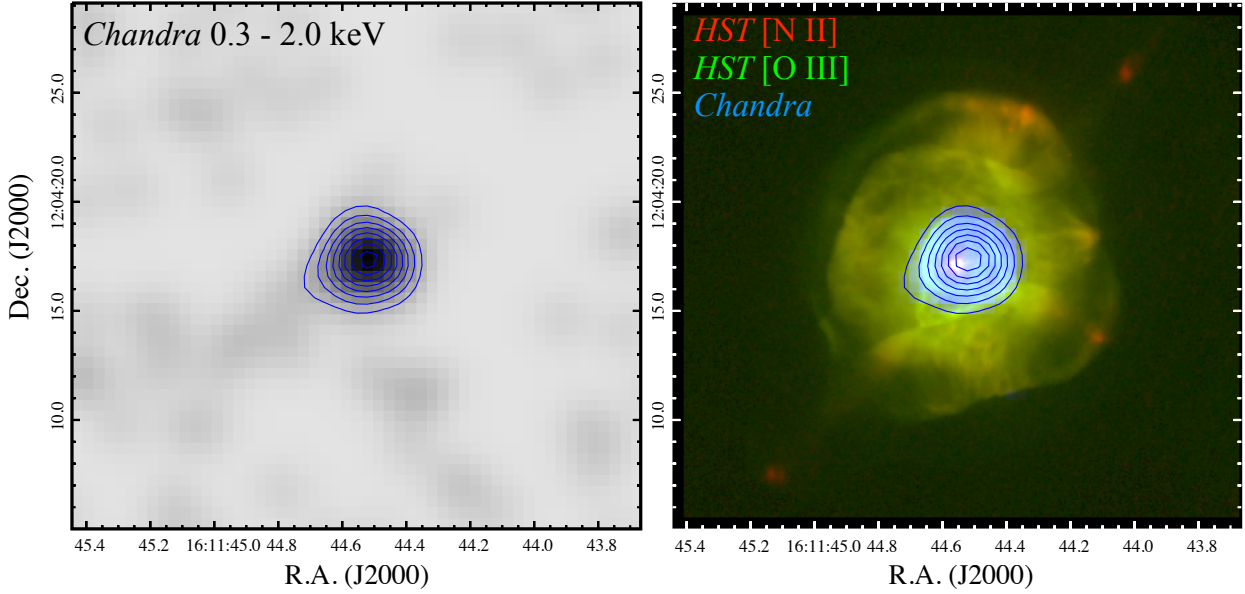


Figure 3. Left: Smoothed *Chandra* ACIS-S image of IC 4593 created for the 0.3–1.5 keV energy range. Right: color-composite optical and X-ray image. The contours correspond to the X-ray emission.

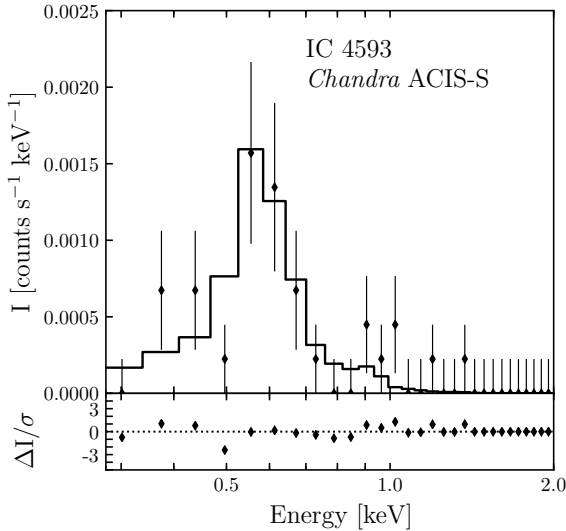


Figure 4. Background-subtracted *Chandra* ACIS-S spectrum of the extended X-ray emission in IC 4593. The error bars correspond to 1σ uncertainty. The solid line plots a model that fits the observed spectrum reasonably well. The bottom panel shows the residuals of the model.

2.3 X-ray emission from the CSPN?

The comparison between the X-ray spectrum of IC 4593 and the *apex* thin-plasma emission model overplotted in Figure 4 reveals some emission excess at ~ 0.4 keV and ~ 0.9 keV. The spatial distribution of the X-ray emission below 0.5 keV is consistent with that of the bulk of X-ray emission, but that of the emission above 0.8 keV shows a remarkable clustering at the position of the CSPN of IC 4593, with 5 photons within a radius of $0''.8$ (Figure 2-left). We have used the `CIAO` task `simulate_psf`, in conjunction with `MARX`

5.5.0 (Davis et al. 2012), to simulate the *Chandra* point spread function (PSF) for a monochromatic spectrum at 1.0 keV at the location of the CSPN of IC 4593. This PSF has been used to run a number of 100,000 Monte Carlo simulations of a detection of 7 counts. It is found that a percentage of these simulations above 95% result in a spatial distribution of the counts that conforms to that shown in the rightmost panel of Figure 2.

The distribution of the X-ray emission with energies above 0.8 keV from IC 4593 thus presents tantalizing evidence for emission from its CSPN. A strong temperature gradient of the X-ray-emitting plasma in the hot bubble might be claimed to produce a similar spatial distribution, but such temperature gradients have not been observed so far in any PN (Yu et al. 2009). Interestingly, the X-ray spectrum of other CSPNe whose hard X-ray emission has been associated with a shock in origin, such as NGC 6543 and NGC 6826, show similar spectral features (Guerrero et al. 2001; Ruiz et al. 2013).

This feature may be indicative of the presence of a plasma with an over-abundance of Ne, or with temperatures $\sim 10^7$ K (as for the CSPN of NGC 6543, Guerrero et al. 2001). Assuming a plasma at this temperature, the count rate above 0.8 keV of 0.09 ± 0.03 counts ks^{-1} , implies an unabsorbed X-ray luminosity in the range $(2\text{--}16) \times 10^{29}$ erg s^{-1} .

3 DISCUSSION

IC 4593 is the farthest PN detected in X-rays by the *Chandra X-ray Observatory*⁴. The detection of X-ray emission from IC 4593 by *Chandra* presented here can be argued to be marginal, but we

⁴ The *Chandra* dramatic decrease of effective area at low energies due to the buildup of a contaminant onto the CCD window may sadly render this record definitive (Guerrero 2020), although we note that there is currently a search of X-ray-emitting PNe in globular clusters using archival *Chandra* data that might result in interesting findings (Montez et al. 2020).

note that the total detected photons (31 ± 6 counts) translates into a $\sigma \approx 5$ detection. Moreover, our results are consistent with other X-ray detections of hot bubbles in PNe: the X-ray emission of IC 4593 is soft with its bulk in the 0.3–1.0 keV energy range, the emission is extended and is confined within the inner rim of the nebula, and the spectral properties of the X-ray-emitting plasma lie within the observed values of other hot bubbles ($T_X \approx 1.7 \times 10^6$ K, $n_e \approx 15 \text{ cm}^{-3}$, and $L_X \approx 10^{30} \text{ erg s}^{-1}$). Furthermore, the presence of a narrow absorption component on the O VI $\lambda 1032 \text{ \AA}$ P Cygni profile of the *FUSE* spectrum reported by Guerrero & De Marco (2013) is suggestive of a conductive or mixing layer between the nebular material and the adiabatically-shocked hot bubble (Iping et al. 2002; Gruendl et al. 2004; Ruiz et al. 2013), which is the main physical mechanism suggested to produce the soft X-ray emission in PNe (Steffen et al. 2008; Fang et al. 2016; Toalá & Arthur 2018).

At a distance of 2.4 kpc, the inner rim of IC 4593 has a physical radius of 0.023 pc, i.e., it harbors one of the most compact hot bubble detected in X-rays together with BD+30°3639, IC 418, and NGC 7027 (Kastner et al. 2012; Freeman et al. 2014).

The spectral properties of the X-ray emission from IC 4593 and especially the spatial distribution of the X-ray emission harder than 0.8 keV are suggestive of a point-source at its CSPN. The X-ray luminosity of this emission implies an X-ray to stellar bolometric luminosity⁵ ratio $\log(L_{X,\text{CSPN}}/L_{\text{bol}})$ in the range between -7.0 and -7.9 . This ratio is consistent with the usual value found for CSPNe dominated by shocks in winds (e.g., Montez et al. 2015, and references therein), in line with the presence of super-ions in the stellar wind of IC 4593 (Herald & Bianchi 2011; Guerrero & De Marco 2013). On the other hand, the X-ray luminosity of the CSPN of IC 4593 is at the upper range for the coronal activity of dwarf late-type stars (see Figure 3 of Guerrero et al. 2019), which would be achieved by an early K or late G dwarf companion with saturated activity ($\log(L_X/L_{\text{bol}}) = -3.56$; Fleming et al. 1995). At the distance of IC 4593, our Sun would have $m_V = 16.73$ mag and $m_K = 15.27$ mag, much weaker than the CSPN of IC 4593, making its optical or near-IR detection unfeasible. Therefore, the current *Chandra* observations cannot be used to assess the origin of this X-ray emission, which cannot be attributed neither to a magnetically active binary companion nor to shocks within its stellar wind. We note, however, that the shocks in the stellar wind of IC 4593 revealed by UV observations would produce X-ray emission at the level and with the spectral properties suggested by the *Chandra* observations presented here.

4 SUMMARY

We present the analysis of *Chandra* ACIS-S3 observations of the PN IC 4593. The observations detect diffuse X-ray emission confined within the inner rim of IC 4593, which would correspond to a hot bubble powered by the wind from its CSPN. Although the number of counts is small, the spectral properties of this X-ray emission are consistent with those of other hot bubbles in PNe, with a temperature $T_X \approx 1.7 \times 10^6$ K and an electron density $n_e = 15 \text{ cm}^{-3}$. The hot bubble of IC 4593 is one of the smallest among PNe, besides BD+30°3639, IC 418, and NGC 7027.

A careful inspection of the hard photons ($E > 0.8$ keV) suggests the presence of a central source very likely associated with

the CSPN. The X-ray luminosity of such a point-source implies a $\log(L_{X,\text{CSPN}}/L_{\text{bol}})$ of -7.4 , very similar to what is observed in CSPNe and OB and Wolf-Rayet stars with self-shocking winds. Alternatively, the X-ray emission can be attributed to an early K or late G dwarf companion, but its presence cannot be confirmed through optical or near-IR observations. Deeper X-ray observations are needed to confirm the presence of an X-ray-emitting CSPN in IC 4593 and to characterise its nature. Such measurements could easily be provided by future X-ray missions as *Lynx* and *Athena*.

ACKNOWLEDGEMENTS

JAT and MAG are supported by the UNAM DGAPA PAPIIT projects IA100318 and IA100720. MAG acknowledges support from grant PGC2018-102184-B-I00, co-funded with FEDER funds. LB and YHC acknowledge support from NASA grant *Chandra* GO2-13024B. YHC acknowledges the research grant 108-2112-M-001-045 from the Ministry of Science and Technology (MOST) of Taiwan. This work has made extensive use of the NASA's Astrophysics Data System. Based on observations made with the NASA/ESA Hubble Space Telescope, and obtained from the Hubble Legacy Archive, which is a collaboration between the Space Telescope Science Institute (STScI/NASA), the Space Telescope European Coordinating Facility (ST-ECF/ESA) and the Canadian Astronomy Data Centre (CADM/NRC/CSA).

REFERENCES

- Arnaud, K. A. 1996, *Astronomical Data Analysis Software and Systems V*, 17
- Bailer-Jones, C. A. L., Rybizki, J., Foesneau, M., et al. 2018, *VizieR Online Data Catalog*, I/347
- Berghefer, T. W., Schmitt, J. H. M. M., Danner, R., et al. 1997, *A&A*, 322, 167
- Cassinelli, J. P., & Olson, G. L. 1979, *ApJ*, 229, 304
- Chu, Y.-H., Guerrero, M. A., Gruendl, R. A., et al. 2001, *ApJ*, 553, L69
- Corradi, R. L. M., Guerrero, M., Manchado, A., et al. 1997, *New Astron.*, 2, 461
- Davis, J. E., Bautz, M. W., Dewey, D., et al. 2012, *Proc. SPIE*, 84431A
- De Marco, O., Bond, H. E., Harmer, D., et al. 2004, *ApJ*, 602, L93
- Dyson, J. E., & Williams, D. A. 1997, *The physics of the interstellar medium*. Edition: 2nd ed. Publisher: Bristol: Institute of Physics Publishing
- Fang, X., Guerrero, M. A., Toalá, J. A., et al. 2016, *ApJ*, 822, L19
- Fleming, T. A., Schmitt, J. H. M. M., & Giampapa, M. S. 1995, *ApJ*, 450, 401
- Fruscione, A., McDowell, J. C., Allen, G. E., et al. 2006, *Proc. SPIE*, 62701V
- Gayley, K. G., & Owocki, S. P. 1995, *ApJ*, 446, 801
- Gruendl, R. A., Chu, Y.-H., & Guerrero, M. A. 2004, *ApJ*, 617, L127
- Guerrero, M. A. 2020, *Proceedings of the Workplans II: Workshop for Planetary Nebula Observations*, eds. T. Ueta and I. Aleman, *Galaxies*, in prep.
- Guerrero, M. A., Toalá, J. A., & Chu, Y.-H. 2019, *ApJ*, 884, 134
- Guerrero, M. A., Chu, Y.-H., Gruendl, R. A., et al. 2001, *ApJ*, 553, L55
- Guerrero, M. A., & De Marco, O. 2013, *A&A*, 553, A126
- Herald, J. E., & Bianchi, L. 2011, *MNRAS*, 417, 2440
- Iping, R. C., Sonneborn, G., & Chu, Y.-H. 2002, *American Astronomical Society Meeting Abstracts* 201, 89.15
- Kastner, J. H., Montez, R., Balick, B., et al. 2012, *AJ*, 144, 58 1997, preprint
- Kastner, J. H., Soker, N., Vrtilik, S. D., et al. 2000, *ApJ*, 545, L57
- Freeman, M., Montez, R., Kastner, J. H., et al. 2014, *ApJ*, 794, 99
- Lucy, L. B., & White, R. L. 1980, *ApJ*, 241, 300
- Miszalski, B., Acker, A., Moffat, A. F. J., et al. 2009, *A&A*, 496, 813
- Montez, R., Kastner, J., Jacoby, G., et al. 2020, *American Astronomical Society Meeting Abstracts* 52, 307.07

⁵ The L_{bol} value derived for the CSPN of IC 4593 from atmosphere model fits by Herald & Bianchi (2011) has been rescaled to the distance used here.

- Montez, R., De Marco, O., Kastner, J. H., et al. 2010, *ApJ*, 721, 1820
Montez, R., Kastner, J. H., Balick, B., et al. 2015, *ApJ*, 800, 8
Montez, R., Kastner, J. H., De Marco, O., & Soker, N. 2005, *ApJ*, 635, 381
Nebot Gómez-Morán, A., & Oskinova, L. M. 2018, *A&A*, 620, A89
O'Connor, J. A., Meaburn, J., López, J. A., et al. 1999, *A&A*, 346, 237
Patriarchi, P., & Perinotto, M. 1995, *A&AS*, 110, 353
Ruiz, N., Chu, Y.-H., Gruendl, R. A., et al. 2013, *ApJ*, 767, 35
Sana, H., Rauw, G., Nazé, Y., et al. 2006, *MNRAS*, 372, 661
Steffen, M., Schönberner, D., & Warmuth, A. 2008, *A&A*, 489, 173
Toalá, J. A., Montez, R., & Karovska, M. 2019, *ApJ*, 886, 30
Toalá, J. A., & Arthur, S. J. 2018, *MNRAS*, 478, 1218
Villaver, E., García-Segura, G., & Manchado, A. 2003, *ApJ*, 585, L49
Villaver, E., Manchado, A., & García-Segura, G. 2012, *ApJ*, 748, 94
Yu, Y. S., Nordon, R., Kastner, J. H., et al. 2009, *ApJ*, 690, 440
Zou, Y., Frank, A., Chen, Z., et al. 2019, *arXiv e-prints*, arXiv:1912.01647
Zucker, D. B., & Soker, N. 1993, *ApJ*, 408, 579